CERES_EBAF_Ed4.1 Data Quality Summary

Version 3
Updated 12/9/2021

Investigation: **CERES**

Data Product: **EBAF**

Data Set: **Terra (Instruments: CERES-FM1 or CERES-FM2)**
                Aqua (Instruments: CERES-FM3 or CERES-FM4)

Data Set Version: **Edition4.1**   **Release Date: June 8, 2021**

CERES Visualization, Ordering and Subsetting Tool: https://ceres.larc.nasa.gov/data/

This document provides a high-level quality assessment of the CERES Energy Balanced and Filled (EBAF) data product. As such, it represents the minimum information needed by scientists for appropriate and successful use of the data product. For a more thorough description of the methodology used to produce EBAF, please see Loeb et al. (2018) and Kato et al. (2018). It is strongly suggested that authors, researchers, and reviewers of research papers re-check this document (especially Cautions and Helpful Hints) for the latest status before publication of any scientific papers using this data product.

Notes to Users:
- A correction has been applied to many variables in EBAF Ed4.1 to mitigate against a spurious drift due to the loss of a microwave humidity sounder in our temperature and humidity reanalysis input data stream, which impacted data months from November 2019 onwards. A detailed description of the correction is provided in Section 2.1. Variables affected include: TOA up longwave clear-sky for the total region, Surface down longwave clear-sky for the total region, Surface net longwave clear-sky for the total region, Surface net total (shortwave+longwave) clear-sky for the total region, TOA longwave cloud radiative effect, TOA net cloud radiative effect, Surface net longwave cloud radiative effect, and Surface net total (shortwave+longwave) cloud radiative effect.
- To ensure you are using the latest version of EBAF, please check the version and release date in the netCDF file you have against the version and release date in this Data Quality Summary.

Changes from EBAF Ed4.0:
- New clear-sky TOA and surface fluxes have been added to Ed4.1. In addition to the clear-sky flux determined only for the cloud-free portions of a region provided in Ed4.0, EBAF Ed4.1 also provides clear-sky flux estimates for the total region, which includes the cloudy portions. These new clear-sky fluxes are defined in a manner that is more in line with how clear-sky fluxes are represented in climate models.
- TOA and surface Cloud Radiative Effects (CREs) in Edition4.1 are determined using the new clear-sky fluxes determined for the total region.

- All-sky SW, LW and net TOA fluxes in Ed4.1 are identical to Ed4.0.
- The entire surface flux record has been reprocessed using consistent Collection 6.1 MODIS aerosols throughout.
- Cloud properties for March 2000 through February 2016 are identical to those in EBAF Ed4.0. For March 2016 onwards, cloud properties are determined using MODIS Collection 6.1 radiances.
- For a more detailed discussion of the differences between EBAF Ed4.1 and EBAF Ed4.0 surface fluxes, please see Section 4.0.

Important Update to Note as of April 8, 2021:
Please see the RED bullet in Cautions and Helpful Hints.

TABLE OF CONTENTS

LIST OF FIGURES

LIST OF TABLES

<u>Table</u>   <u>Page</u>

1.0   Introduction

The CERES Energy Budget and Filled (EBAF) dataset is produced using measurements from several instruments. It involves CERES and MODIS instruments flying on the Terra (descending sun-synchronous orbit with an equator crossing time of 10:30 A.M. local time) and Aqua (ascending sun-synchronous orbit with an equator crossing time of 1:30 P.M. local time) as well as geostationary imagers that provide hourly diurnal information between 60°S-60°N. Each CERES instrument measures filtered radiances in the shortwave (SW; wavelengths between 0.3 and 5 μm), total (TOT; wavelengths between 0.3 and 200 μm), and window (WN; wavelengths between 8 and 12 μm) regions. Unfiltered SW, longwave (LW) and WN radiances are determined following Loeb et al. (2001) and radiance-to-flux conversion uses empirical Angular Distribution Models from Su et al. (2015). CERES instruments provide global coverage daily, and monthly mean regional fluxes are based upon complete daily samples over the entire globe. Cloud properties are determined from MODIS and geostationary imager measurements (Minnis et al. 2020).

Despite recent improvements in satellite instrument calibration and the algorithms used to determine SW and LW outgoing top-of-atmosphere (TOA) radiative fluxes, a sizeable imbalance persists in the average global net radiation at the TOA from CERES satellite observations. With the most recent CERES Instrument calibration improvements, the SYN1deg_Edition4 net imbalance is ~4.3 W m^{-2}, much larger than the expected observed ocean heating rate ~0.71 W m^{-2} (Johnson et al. 2016). This imbalance is problematic in applications that use Earth Radiation Budget (ERB) data for climate model evaluation, estimations of the Earth's annual global mean energy budget, and studies that infer meridional heat transports. *The EBAF dataset uses an objective constrainment algorithm to adjust SW and LW TOA fluxes within their ranges of uncertainty to remove the inconsistency between average global net TOA flux and heat storage in the Earth-atmosphere system.*

A second problem users of standard CERES Level-3 data products have noted is the occurrence of gaps in monthly mean clear-sky TOA flux maps due to the absence in some 1°x1° regions of cloud-free areas occurring at the CERES footprint scale (~20-km at nadir). As a result, clear-sky maps from CERES SSF1deg contain many missing regions. In EBAF, the problem of gaps in clear-sky TOA flux maps is addressed by inferring clear-sky fluxes from both CERES and Moderate Resolution Imaging Spectrometer (MODIS) measurements to produce a clear-sky TOA flux in each 1°x1° region every month.

EBAF Ed4.1 introduces a new clear-sky flux parameter. In addition to the clear-sky flux determined only for the cloud-free portions of a region provided in Ed4.0, EBAF Ed4.1 also includes clear-sky flux estimates for the total region, which includes the cloudy portions. These new clear-sky fluxes are defined in a manner that is more in line with how clear-sky fluxes are represented in climate models. ***These new clear-sky fluxes are used to determine Cloud Radiative Effect (CRE) in Edition4.1.***

This document provides a brief description of the new features introduced in EBAF Ed4.1 product, which now merges TOA and surface fluxes into one product. For detailed descriptions of how TOA and surface radiative fluxes in EBAF are generated, please see Loeb et al. (2018) and Kato et al. (2018). Loeb et al. (2020) describes the methodology used to determine the new clear-sky flux estimates for total regions. We briefly summarize the methodology in Section 2.0. Section 3.0 briefly discusses cloud properties provided in EBAF Ed4.1 while Section 4.0 summarizes the differences between Ed4.1 and Ed4.0. In Section 5.0, Cautions and Helpful Hints are provided and Section 6.0 discusses Accuracy and Validation of the EBAF product.

2.0   Clear-Sky Flux Estimate for Total Region

We derive a regional monthly adjustment factor (Δ^C) to the EBAF observed regional monthly mean clear-sky flux (F_{cs}^O) as follows:

$$F_{cs}^o(CldRem) = F_{cs}^o + \Delta^C \tag{1}$$

where

$$\Delta^C = F_{cs}^C(CldRem) - F_{cs}^C(ObsWgt) \tag{2}$$

$F_{cs}^C(CldRem)$ corresponds to radiative transfer model flux calculations over a gridbox determined by ignoring clouds in the atmospheric column. The flux calculations are initialized using satellite-derived cloud and aerosol properties, and temperature and specific humidity profiles from reanalysis. $F_{cs}^C(CldRem)$ calculations are made hourly, averaged monthly, and are a standard output of the CERES SYN1deg Ed4.1 data product (Rutan et al. 2015; Kato et al. 2018). In CERES SYN1deg Ed4.1, temperature, specific humidity, and ozone profiles are from the NASA Goddard Earth Observing System version 5.4.1 (GEOS- 5.4.1) reanalysis (Rienecker et al. 2008). Aerosol data are based upon the Model of Atmospheric Transport and Chemistry (MATCH; Collins et al. 2001), which assimilates Moderate Resolution Imaging Spectroradiometer (MODIS) aerosol optical depth and provides hourly aerosol optical depths and aerosol type. Surface albedo and emissivity input data used in the radiative transfer model calculations are described in detail in Rutan et al. (2015).

$F_{cs}^C(ObsWgt)$ is the calculated clear-sky flux over a gridbox weighted by observed clear-sky fraction. It is derived from hourly $F_{cs}^C(CldRem)$ in SYN1deg Ed4.1 weighted by MODIS clear-sky fraction. The clear-sky fraction weights are derived by sorting instantaneous CERES footprint clear-sky fractions from the CERES Single Scanner Footprint (SSF) TOA/Surface Fluxes and Clouds Ed4.1 product into 1°×1° regions. Clear-sky fractions within CERES footprints are determined by applying a cloud mask to each MODIS pixel and classifying it as clear or cloudy (Trepte et al. 2019). To produce hourly clear-sky fraction weights, the clear-sky fractions are temporally interpolated for Terra-only observation times prior to July 2002 and both Terra and Aqua observation times from July 2002 onward. The monthly mean $F_{cs}^C(ObsWgt)$ is determined by first calculating monthly hourly averages and then averaging the monthly hourly means. In the SW, $F_{cs}^C(ObsWgt)$ is normalized by the ratio of the TOA insolation for complete temporal sampling over a month to that corresponding to clear-sky-weighted temporal sampling. This ensures that Δ^C is not impacted by a diurnal cycle sampling bias due to the clear-sky weighting.

Because the early part of the record relies on Terra-only (March 2000 – June 2002) and the remainder uses both Terra and Aqua, an adjustment is applied to the Terra-only part of the record in order to minimize any discontinuities between these two periods. A discontinuity can arise because observations during the Terra-only period are only available twice daily compared to four times daily during the combined Terra-Aqua period and because of differences in the character of the cloud masks applied to Terra and Aqua MODIS data. Both can cause differences in clear-sky sampling and introduce a discontinuity. To mitigate this, we apply adjustments to the Terra-only part of the record determined from the difference between climatological monthly mean values of $F_{cs}^C(ObsWgt)$ for Terra and Aqua combined and Terra-only. We use a 10-year period between July 2005 and June 2015 to derive the adjustments for each calendar month.

The above procedure producing $F_{cs}^o(CldRem)$ is essentially the same at TOA and at the surface. In both cases, TOA and surface $F_{cs}^C(ObsWgt)$ are adjusted by the similar method used for the all-sky adjustment before Eq. (1) is applied. The adjustment process for EBAF TOA and surface clear-sky fluxes are described in Loeb et al. (2018) and Kato et al. (2018), respectively.

The regional distribution of Δ^C for seasonal months averaged over 10 years (07/2005-06/2015) is shown in Figure 2-1a-d for TOA LW and Figure 2-2a-d for TOA SW. In the LW, the Δ^C adjustment is generally negative throughout the year in the tropics and mid-latitudes and is positive at high latitudes during winter, spring, and fall, and near zero during summer. The most pronounced values occur during January over Australia, reaching -12 W m^{-2}, and over Greenland, reaching 18 W m^{-2} (Figure 2-1a). The overall global mean LW Δ^C for the entire 07/2005-06/2015 period is –2.2 W m^{-2} and the standard deviation is 0.15 W m^{-2} based upon the 120 monthly mean global values.

In the tropics the spatial pattern of Δ^C is closely tied to the pattern of upper tropospheric humidity and cirrus. Regions with elevated upper tropospheric humidity and cirrus lower the monthly mean LW $F_{cs}^C(CldRem)$ compared to $F_{cs}^C(ObsWgt)$, which favors drier and less cloudy conditions. Δ^C adjustments are pronounced in the west tropical Pacific, South Convergence Zone (SPCZ) and Intertropical Convergence Zone (ITCZ) and are closer to zero over the stratocumulus regions off the west coasts of North and South America, Africa, and Australia. The Δ^C adjustment at high latitudes is positive most of the time because in the presence of cloud, surface and boundary layer temperatures tend to be warmer than cloud-free conditions, resulting in larger LW fluxes for $F_{cs}^C(CldRem)$ compared to $F_{cs}^C(ObsWgt)$. This effect is particularly strong over Greenland during January.

In the SW, Δ^C remains near-zero over large portions of the ice-free oceans, and ranges between 1 and 3 W m^{-2} over the North Pacific and North Atlantic Oceans during April and July (Figure 2-2b and Figure 2-2c) as well as parts of the Southern Ocean in January and October (Figure 2-2a and Figure 2-2d). Δ^C values reach 5 W m^{-2} during July over the Bay of Bengal during the Indian Monsoon as well as over the northern part of the Arabian Sea (Figure 2-2c). Over land, Δ^C is large over eastern China all year round, reaching 12 W m^{-2} in April. Appreciable negative values of Δ^C occur over parts of northern Russia and eastern Canada during April. When averaged globally, the overall mean SW Δ^C for the entire 07/2005-06/2015 period is 0.47 W m^{-2} and the standard deviation is 0.16 W m^{-2} based upon the 120 monthly mean global values.

Over snow-free land surfaces, the SW Δ^C adjustment tends to be positive because the cloudier days tend to have larger aerosol optical depths, resulting in larger $F_{cs}^C(CldRem)$ monthly mean values. The larger aerosol optical depths on cloudier days could be due to higher aerosol loadings and because aerosol optical depth increases with relative humidity (Clarke et al., 2002). Another contributing factor could be from biases in the MODIS clear-sky weights. During days with heavy aerosol loadings over land, discriminating between clear and cloudy imager pixels is extremely challenging. If there is a tendency to misidentify heavy aerosol as cloud, this will bias the $F_{cs}^C(ObsWgt)$ value low, resulting in a positive SW Δ^C adjustment. Over northern hemisphere land regions with seasonal snow cover (e.g., in April), we suspect there may be a correlation between snow and cloud cover. For example, if the cloud cover is lower when the surface is covered with snow, the clear-sky weighting will assign more weight to the days of the month when the surface is snow covered, leading to a larger monthly mean for $F_{cs}^C(ObsWgt)$ and a negative SW Δ^C adjustment. The reason for a correlation between snow and cloud cover may be physical or it could also result from inconsistent cloud identification between snow and snow-free covered

days. If the cloud mask algorithm tends to misidentify cloud over snow as cloud-free, this could cause $F_{cs}^{C}(ObsWgt)$ to be biased high, resulting in a negative SW Δ^{C} adjustment. However, preliminary comparisons with the Cloud-Aerosol Lidar and Infrared Pathfinder Satellite Observation (CALIPSO; Winker et al. 2010) show no evidence that the MODIS cloud mask misidentifies clouds over snow as cloud-free (Yost et al. 2020).
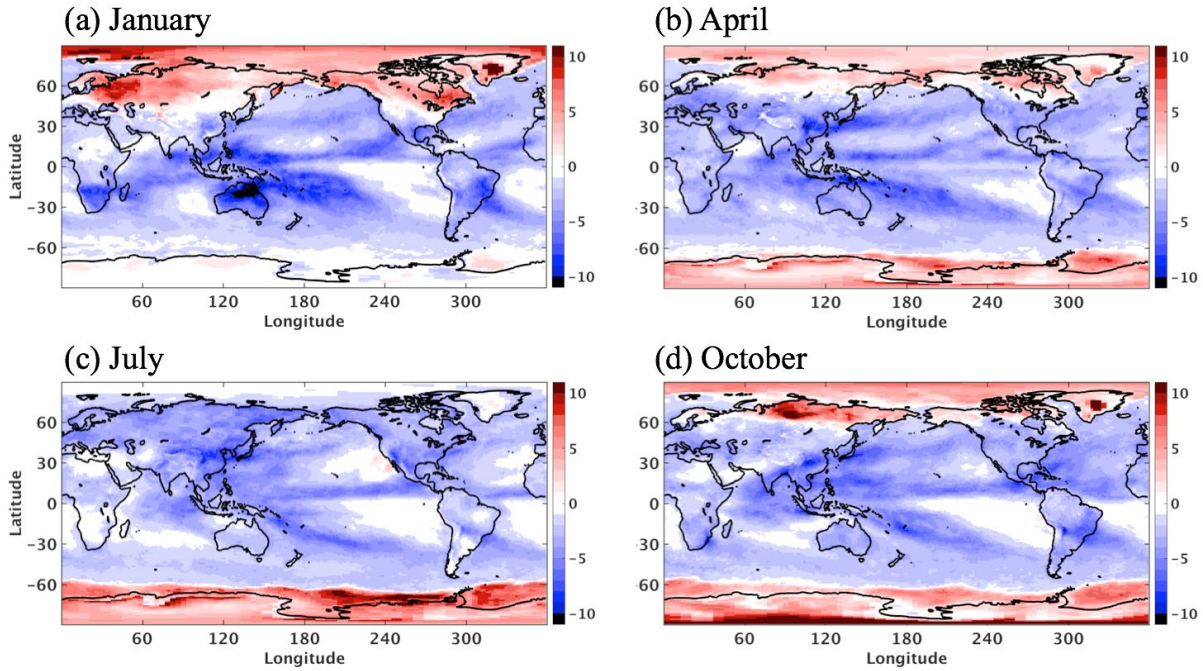
Figure 2-1. TOA LW adjustment (Δ^{C}) for: (a) January, (b) April, (c) July and (d) October based upon 10-year climatology of CERES EBAF data for 07/2005-06/2015. (Units: W m^{-2})
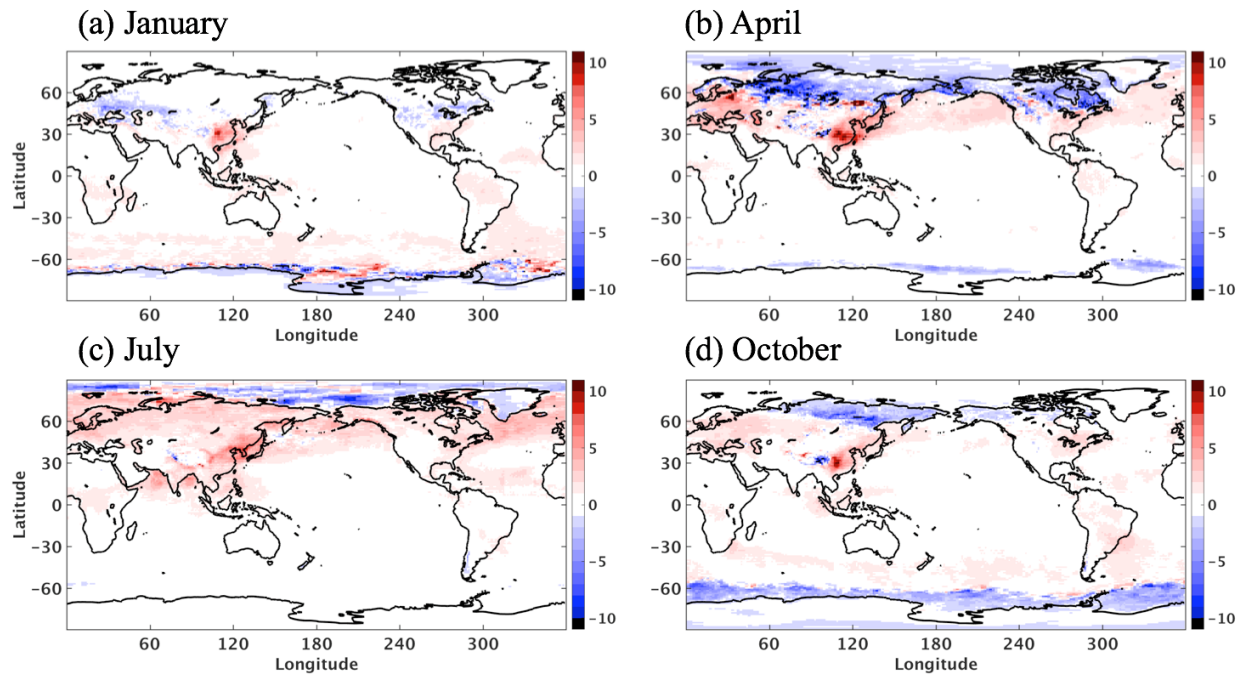
Figure 2-2. Same as Figure 2-1 but for TOA SW Δ^C. (Units: W m^{-2})

        To get a sense of how robust the SW and LW adjustment factors are to the meteorological assimilation system used, adjustment factors determined using SYN1deg clear-sky TOA fluxes were compared with those from MERRA-2, ERA-Interim and ERA5 for one month (January 2008). In each case, the same MODIS-based clear area weights were used. In the LW, the 1° regional RMS difference between adjustment factors from the different reanalyses and SYN1deg was < 1 W m^{-2}. Differences were generally between -3 to -1 W m^{-2} over the Arctic Ocean, likely due to skin temperature differences amongst the various datasets. In the SW, regional RMS differences were twice as large as for LW due primarily to discrepancies in regions of heavy aerosol and sea-ice off of Antarctica. For non-polar ocean regions, regional RMS differences were < 1 W m^{-2}. A more detailed description of these comparisons is provided in Loeb et al. (2020). Also included in that paper are comparisons of CERES Cloud Radiative Effect (CRE) determined with the new clear-sky fluxes and CREs from seven CMIP6 historical simulations.

        Global 10-year global mean TOA and surface clear-sky fluxes with and without the Δ^C adjustment are provided in Table 2-1. In the LW, the Δ^C adjustment results in a 2.2 W m^{-2} reduction in TOA flux compared to the case in which no adjustment is applied. In the SW, the adjustment causes a 0.5 W m^{-2} increase. At the surface, the Δ^C adjustment enhances clear-sky downward LW flux by 3.3 W m^{-2} and reduces clear-sky downward SW flux by 2.3 W m^{-2}. The positive difference in the LW is due to the tendency for moister conditions under cloudy conditions, resulting in enhanced downward clear-sky flux after removing the clouds in the calculation. In the SW, the higher humidity and aerosol concentration has the opposite effect.

        For additional information about the new CERES clear-sky fluxes, please see the following presentation:
https://ceres.larc.nasa.gov/documents/STM/2019-05/12_Loeb_EBAF_Talk_Spring2019.pdf

Table 2-1. Global mean clear-sky fluxes for July 2005-June 2015 (W m^{-2}).

		EBAF (No Adjustment)	EBAF with Δ^c Adjustment	Difference
Clear-Sky TOA	LW	268.1	265.9	-2.2
	SW	53.3	53.8	0.5
	Net	18.6	20.3	1.7
Clear-Sky Surface	LW down	313.9	317.2	3.3
	LW up	397.6	398.2	0.6
	LW Net	-83.7	-81.0	2.7
	SW down	243.0	240.7	-2.3
	SW up	29.5	29.1	-0.4
	SW Net	213.5	211.6	-1.9
	SW + LW Net	129.8	130.6	0.8

2.1   Mitigation of Humidity and Temperature Drift in GEOS-5.4.1 (November 2019 onwards)

Loss of the Microwave Humidity Sounder (MHS) has caused a spurious drift in specific humidity and temperature in the GEOS-5.4.1 reanalysis data used by CERES for data months from November 2019 onwards. The drift causes the entire troposphere (surface to 100 hPa) to become too moist, which leads to a drift in TOA LW Δ^C. To mitigate the impact of the drift, we use MERRA-2 temperature and specific humidity anomalies from November 2019 onward to derive a correction. Unlike GEOS-5.4.1, loss of MHS has little impact on MERRA-2. The correction involves first calculating monthly mean total area minus clear-sky fraction weighted profiles of temperature and specific humidity in each 1°×1° region for GEOS-5.4.1 and MERRA-2. Next, we calculate the MERRA-2 minus GEOS-5.4.1 differences of these quantities. The differences are then scaled by temperature and humidity radiative kernels to provide temperature and humidity corrections ($\Delta^c_{correction}(\Delta T)$ and $\Delta^c_{correction}(\Delta q)$, respectively), which are used to adjust the TOA upward and surface downward longwave Δ^c as follows:

$$\Delta^c_{new} = \Delta^c_{old} + \Delta^c_{correction}(\Delta T) + \Delta^c_{correction}(\Delta q)$$

where Δ^c_{old} is based upon the original GEOS-5.4.1 Δ^c correction. The radiative kernals provide an efficient way of relating differences in temperature and humidity to either TOA or surface flux. Figure 2-3 and Figure 2-4 provide a time series of TOA LW and surface downward LW total area clear-sky flux before and after applying the correction.

The variables in EBAF Ed4.1 that are affected by the correction are: TOA up Longwave clear-sky total region, Surface down longwave clear-sky total region, Surface net longwave clear-sky total region, Surface net total (shortwave+longwave) clear-sky total region, TOA Longwave cloud radiative effect, TOA net cloud radiative effect, Surface net longwave cloud radiative effect, and Surface net total (shortwave+longwave) cloud radiative effect.

MTH_GLB_LWTOAUP_CLEAR_CLDREM_OBSWGT

$\mu=-2.153$ $\mu=-2.133$ $\Delta\mu=-0.019$ $\rho= 0.905$

MTH_GLB_LWTOAUP_CLEAR_CLDREM_OBSWGT Anomaly

$\sigma= 0.126$ $\sigma= 0.135$ $-0.112_{/decade}$ $-0.061_{/decade}$ $\rho_{anomaly}= 0.834$
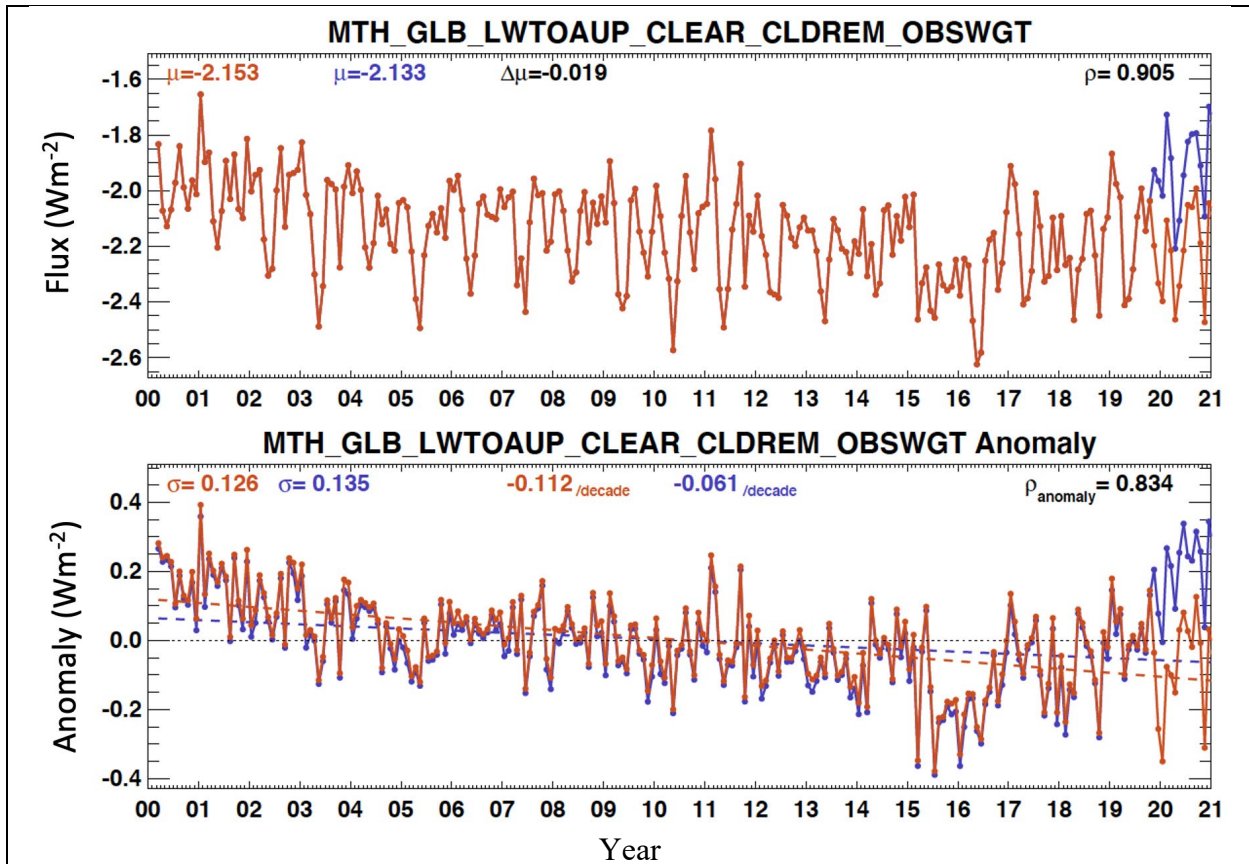
Figure 2-3. Top) Time series of the difference of global monthly mean TOA longwave flux with cloud removed and averaged by weighting by observed clear-sky fraction Δ^c. The blue line is computed with GEOS-5.4.1 temperature and specific humidity profiles, and the red line is TOA longwave flux MERRA-2. Bottom) monthly deseasonalized anomaly time series of the top plot.
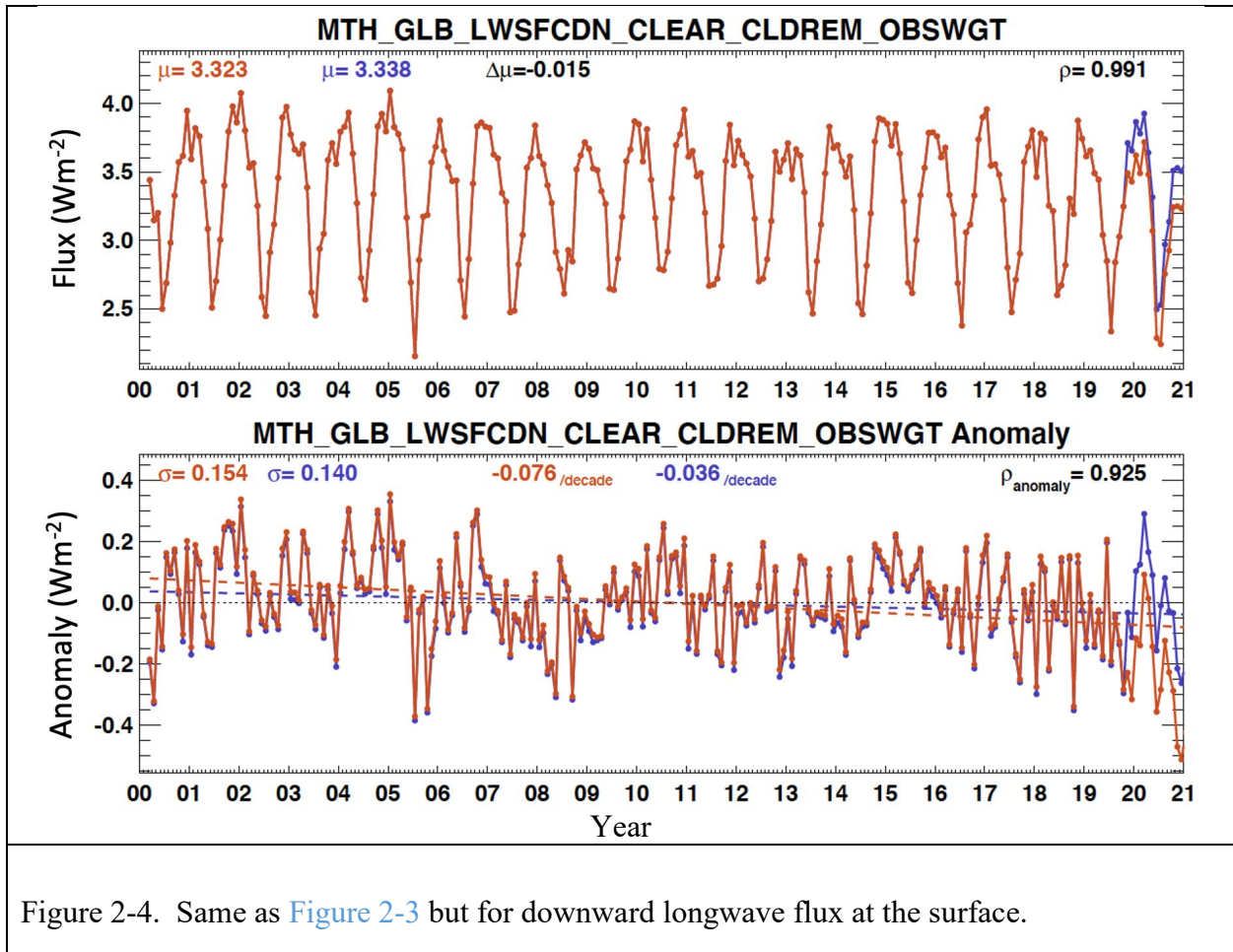
Figure 2-4. Same as Figure 2-3 but for downward longwave flux at the surface.

3.0   Cloud Properties

EBAF-TOA Ed4.0 provides MODIS-based monthly mean cloud properties alongside TOA fluxes. The cloud properties include cloud amount, optical depth, effective pressure, and temperature derived from instantaneous cloud retrievals averaged over CERES footprints provided in the CERES SSF Ed4 product. The instantaneous cloud properties in SSF Ed4 are based upon an updated methodology to that described in Minnis et al. (2011). For a description of the methodology and accuracy of instantaneous cloud properties in CERES SSF Ed4, please refer to the SSF Ed4.0 Data Quality Summary:

https://asdc.larc.nasa.gov/documents/ceres/quality_summaries/CER_SSF_Terra-Aqua_Edition4A.pdf

In EBAF Ed4.0, the cloud optical depths are based upon daytime MODIS retrievals only, while the remaining cloud properties are computed using both daytime and nighttime data. The monthly mean cloud properties between March 2000 and June 2002 are retrieved from Terra-MODIS, while cloud properties from July 2002 onwards are determined from the average of Terra-MODIS and Aqua-MODIS. Because the Terra-MODIS cloud properties represent the cloud conditions observed during the Terra sun-synchronous orbit overpass time of 10:30 a.m. local equator crossing time, they may differ substantially over maritime stratus and land afternoon convection compared to those during the Terra-Aqua period. As a result, some of the cloud properties may exhibit a discontinuity in some regions in July 2002.

To determine monthly mean cloud properties, we follow the same steps as in the CERES SSF1deg data product. The instantaneous cloud properties in the SSF product are spatially averaged into 1° regions. These are then linearly interpolated hourly to estimate cloud conditions between the MODIS-observed measurements. The hourly regional cloud properties, whether observed or interpolated, are then averaged over the month. While cloud fraction is simply averaged, the remaining cloud properties are weighted by cloud fraction. Cloud optical depth is averaged in log form since log cloud optical depth is approximately proportional to visible radiance. The monthly regional cloud properties within a 1° latitude zone are averaged to compute the zonal mean. The global mean cloud properties are averaged from the zonal means using geodetic weighting.

Because the Aqua MODIS 1.6 μm channel failed shortly after launch, the 1.24 μm channel is used as an alternative in both Aqua and Terra Ed4 daytime cloud optical depth retrievals over snow. However, the 1.24 μm channel is not optimal for cloud optical depth since surface reflectance can affect retrievals more than the 1.6 μm channel. Surface shortwave downward flux validation of radiative transfer results over Dome C using 1.6 μm and 1.24 μm cloud retrievals anecdotally suggest that the 1.24 μm cloud optical depths over snow are too large by several percent.

Users interested in a more extensive set of cloud properties at hourly, daily, monthly, and monthly hourly timescales are encouraged to consider the SSF1deg or SYN1deg data products, available on the CERES Visualization, Ordering and Subsetting tool: (https://ceres.larc.nasa.gov/data/).

4.0   Differences Between EBAF Ed4.1 and EBAF Ed4.0

As noted in Section 2.0, a major change in EBAF Ed4.1 is the introduction of new clear-sky TOA and surface fluxes for the total region. These are provided in addition to the previous clear-sky fluxes defined only from the cloud-free portions of a region. **However, rather than providing two sets of CREs, EBAF Ed4.1 only calculates one set of CREs, using the new clear-sky fluxes.** *All-sky TOA fluxes in EBAF Ed4.1 did not change from those in EBAF Ed4.0.*

There are two other reasons requiring an Ed4.1 release of EBAF. The first reason is to incorporate Collection 6.1 MODIS calibration changes. Following a slow degradation that started around 2008, radiances for two channels of MODIS on Terra (6.7µm and 8.6µm) drastically jumped in March 2016. The MODIS team released Collection 6.1 data products with corrections applied to these channels in spring 2018. To account for the large discontinuity in March 2016, cloud properties in the CERES SSF product for March 2016 onward have been reprocessed with Collection 6.1 MODIS calibration (Figure 4-1). These two channels are used to detect nighttime clouds over snow and sea ice covered surfaces in the CERES cloud algorithm. Because the reprocessing with Collection 6.1 MODIS only starts in 2016, there is a drift in nighttime cloud fraction for MODIS-Terra over permanent snow and sea ice surface starting in 2008. The difference in the monthly mean cloud fraction averaged over snow and sea ice surfaces can be as large as 0.1. A detailed description of the method used to mitigate the impact of the degradation on surface fluxes is given here in Section 2.1.1.4 of
https://ceres.larc.nasa.gov/documents/DQ_summaries/CERES_EBAF-Surface_Ed4.1_DQS.pdf.

Figure 4-2 shows the difference (Edition 4.1 minus Edition 4.0 EBAF) of monthly mean all-sky downward longwave fluxes for March 2003-September 2018. Differences primarily occur over polar regions during polar night caused by the difference in the nighttime cloud fraction derived from MODIS on Terra.

The second reason is to correct an error in Collection 5 MODIS-retrieved aerosol optical thicknesses used in Edition4.0. In CERES processing, MODIS aerosol optical thicknesses are assimilated into an aerosol transport model (MATCH), which are then used to compute surface radiative fluxes. The MODIS Collection 5 aerosol retrieval error primarily affects aerosol optical thickness over land. Differences are larger over Amazon, tropical western Pacific, and central Africa (Figure 4-3, top). To overcome this problem, the CERES team reprocessed the entire SYN1deg record using consistent Collection 6.1 MODIS (Terra and Aqua) aerosol optical thicknesses in Edition 4.1. Figure 4-3 (bottom) shows the difference in monthly mean clear-sky downward surface shortwave fluxes between Ed4.1 and Ed4.0. In regions in which aerosol optical thickness differences are large, monthly regional mean clear-sky downward shortwave flux differences can be greater than 10 W m^{-2}, While the problem in Collection 5 MODIS only affects the aerosol optical thickness over land, spatial interpolation and filling in MATCH leads to differences over ocean as well. The large standard deviations of downward shortwave flux over the Arctic is caused by the seasonal difference in the aerosol optical thickness. Larger differences in the aerosol optical thickness in the Arctic occur during summertime.

Another cause of differences between surface radiative fluxes in EBAF Ed4.1 and Ed4.0 is due to cloud property retrieval algorithm changes specifically for the Himawari-8 GEO imager, which covers the western Pacific from July 2015 onward. As shown in Figure 4-4, all-sky downward longwave flux differences occur near Australia between 90°E-180°E. Differences in downward shortwave flux over land are due to the difference in the aerosol optical thickness discussed above. Differences in the downward longwave flux over the Antarctic are due to the differences in cloud fraction resulting from MODIS calibration changes.

For additional information about EBAF Ed4.1 surface fluxes, please see the following presentation: https://ceres.larc.nasa.gov/documents/STM/2019-05/11_kato_etal_sarb_update.pdf

Parameter	ED4.0	ED4.1
MODIS-collection	Terra-MODIS 6.7, 8.6 μm striping, March 2016 to March 2018	MODIS C6.1 resolved the Terra-MODIS 6.7, 8.6 μm striping
MATCH-Edition	Large discontinuity between MODIS C5 & C6.1 AOD inputs	Uses MODIS C6.1 AODs as input for entire CERES record
MODIS Clouds	Impacted Terra cloud properties	Terra cloud properties corrected beginning in Feb 2016
GEO Clouds	Him-8, GOES-16,17, Met-8,11 cloud codes with bugs	Consistent cloud code using MATCH Ed4.1, begin July 2015
Surface fluxes	The clear-sky SW down surface flux was impacted by MODIS C5 & C6.1 AOD discontinuity	SYN surface fluxes, computed using consistent GEO cloud code with MATCH Ed4.1 and tuned fluxes to correct GEO TOA flux

Figure 4-1. Timeline of MODIS collection and MATCH aerosols used in Edition 4.0 and 4.1 EBAF data products. Edition 4.0 MATCH uses MODIS collection 5 and 6 aerosols. Edition 4.0 EBAF-surface was produced from March 2000 through March 2018. Collection 6.1 aerosols are used in MATCH 4.1.
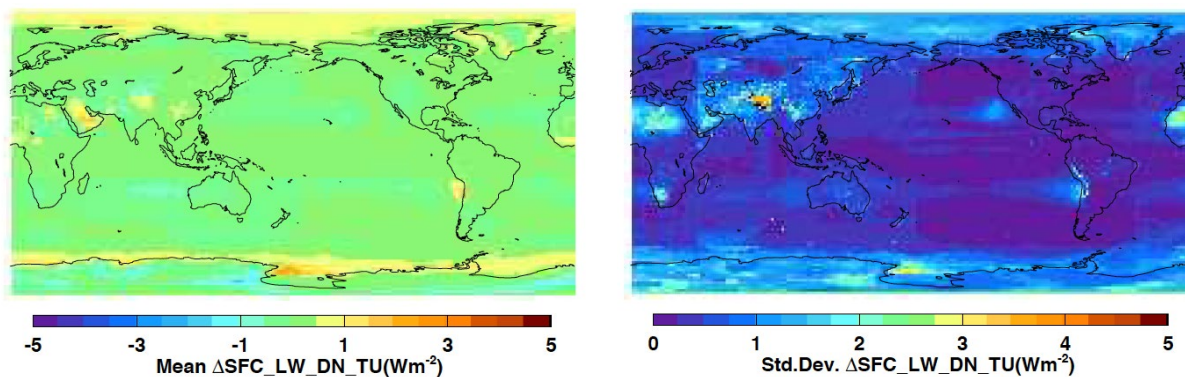
Figure 4-2. Monthly mean all-sky downward surface longwave flux difference (Edition 4.1 minus Edition 4.0 MATCH) averaged from March 2003 through September 2018 on the left and standard deviation the monthly mean differences on the right.
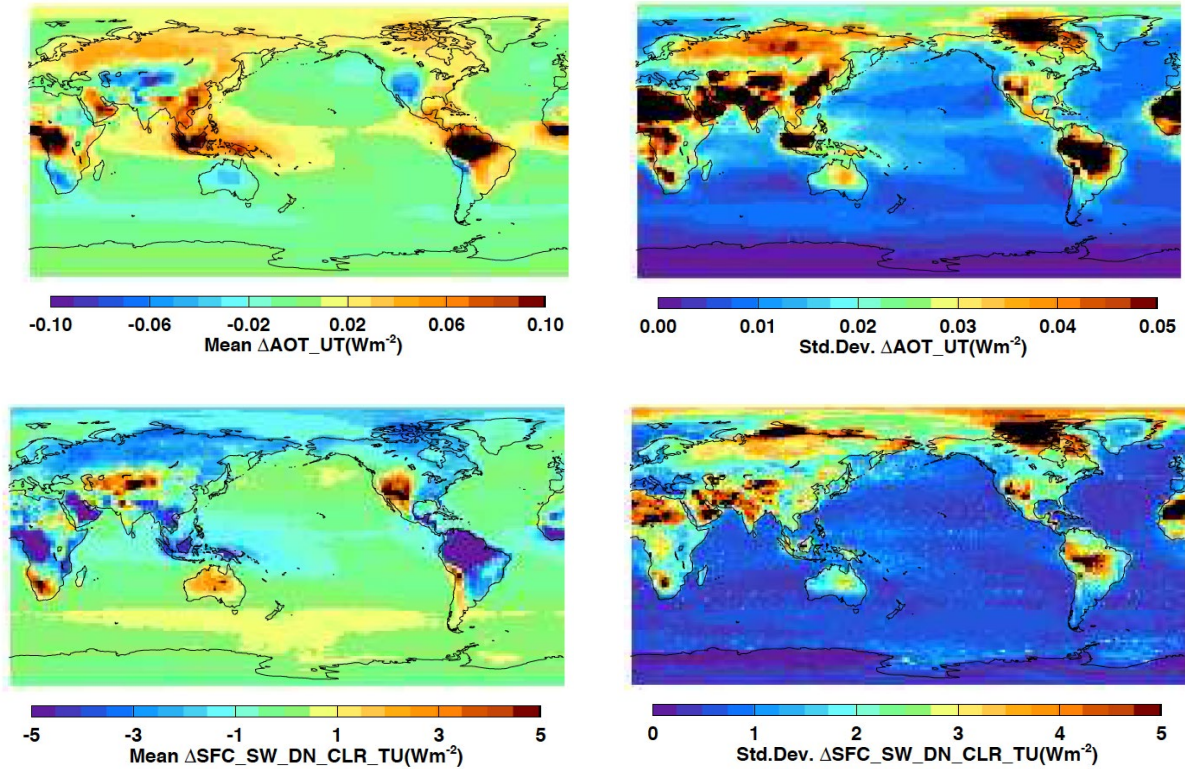
Figure 4-3. Top: Monthly mean aerosol optical thickness difference (Edition 4.1 minus Edition 4.0 MATCH) averaged from March 2003 through September 2018 (left) and standard deviation of the monthly mean differences (right). Bottom: Corresponding difference in monthly mean clear-sky downward surface shortwave flux (Edition 4.1 minus Edition 4.0) (left) and standard deviation the monthly mean differences (right). Clear-sky in bottom plots is defined for cloud-free portions of a region, consistent with approach used in EBAF Ed4.0.
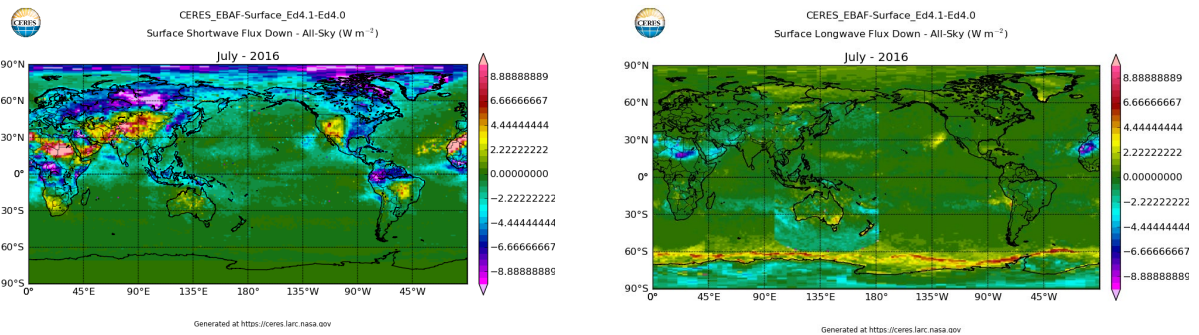
Figure 4-4. Difference of monthly mean all-sky downward shortwave (left) and longwave (right) flux for July 2016.

4.1   Global mean flux difference between Edition 4.0 and 4.1

Table 4-1 compares global mean TOA and surface fluxes for Ed4.0 and Ed4.1, averaged from July 2005 to June 2015. As noted earlier, TOA all-sky fluxes are identical in EBAF Ed4.1 and EBAF Ed4.0. At the surface, slight differences are observed for SW, mainly due to changes in aerosols used in the calculations. Larger differences are seen in CRE due to the use of clear-sky fluxes defined over the total region in EBAF Ed4.1. In EBAF Ed4.1, LW CRE is changed by -2.1 W m^{-2} at the TOA and -2.6 W m^{-2} at the surface. The TOA SW CRE difference is much smaller (0.5 W m^{-2}), so that the magnitude of the total CRE remains appreciable (-1.7 W m^{-2}). At the surface, there is greater compensation between SW and LW CRE differences, resulting in a smaller total CRE change (-0.6 W m^{-2}).

Table 4-1. Global mean TOA and surface fluxes and CREs for EBAF Edition 4.1 and Edition 4.0 for July 2005 to June 2015 (W m^{-2}).

|	**All-sky**	**Ed4.0**	**Ed4.1**	**Ed4.1 – Ed4.0**
	SW insolation	340.0	340.0	0.0
TOA	SW up	99.1	99.1	0.0
	LW u p	240.1	240.1	0.0
	TOT Net	0.71	0.71	0.0
	SW down	187.1	186.6	-0.5
	SW up	23.3	23.2	-0.1
	SW Net	163.7	163.3	-0.4
Surface	LW down	344.8	344.8	0.0
	LW up	398.3	398.3	0.0
	LW net	-53.5	-53.5	0.0
	TOT net	110.2	109.8	-0.4
	CRE	**Ed4.0**	**Ed4.1**	**Ed4.1 – Ed4.0**
	SW	-45.8	-45.3	0.5
TOA	LW	27.9	25.8	-2.1
	TOT	-17.9	-19.6	-1.7
	SW	-50.2	-48.2	2.0
Surface	LW	30.0	27.4	-2.6
	TOT	-20.2	-20.8	-0.6

5.0   Cautions and Helpful Hints

The CERES Science Team notes several CAUTIONS and HELPFUL HINTS regarding the use of CERES_EBAF_Ed4.1:

- TOA and surface Cloud Radiative Effects (CREs) in EBAF Ed4.1 are determined using the new clear-sky fluxes determined for the total region. This differs from EBAF Ed4.0, which determined CRE using clear-sky fluxes determined from cloud-free portions of a region only.
- The CERES_EBAF_Ed4.1 product can be visualized, subsetted, and ordered from: https://ceres.larc.nasa.gov/data/.
- For orders exceeding 2 GB, users are encouraged to use the Shopping Cart feature on the "Subsetting and Browse" page ("Add to Cart"). The data will be made available for download.
- The Aqua satellite experienced an anomaly preventing any data transmittal from August 16 to September 3, 2020. CERES processing filled this Aqua gap with the SSF NOAA-20 Ed1B fluxes and clouds from August 16-31. September 1-3 was not filled.
- Global means are determined using zonal geodetic weights. The zonal geodetic weights can be obtained from (https://ceres.larc.nasa.gov/data/general-product-info/#geodetic-zone-weights-information).
- Climatological mean values used to calculate deseasonalized monthly anomalies are determined for a base period of July 2005 – June 2015.

(a) TOA Fluxes:

- Users are cautioned that all-sky SW and LW TOA fluxes are determined from Terra only from March 2000-June 2002 and combined Terra and Aqua for July 2002 onwards. Clear-sky TOA fluxes are derived from Terra prior to July 2002 and Aqua thereafter. An adjustment is applied to clear-sky fluxes during the Terra-only period to remove first-order differences between Terra and Aqua. Consequently, uncertainties are slightly larger prior to July 2002.
- The solar incoming TOA flux is derived from daily SORCE TIM measurements, which have an average annual flux of ~1361 W m^{-2} vary with time and take into account the solar sunspot cycle with an amplitude of ~0.1%.
- A processing glitch was discovered in the daily TSI file. The TSI daily fluxes during August 2019 and May through November 2020 (shown as the red values in Figure 5-1) were found to be scaled incorrectly resulting in a daily flux that was biased by ~ +0.8 W m^{-2}. The incorrect daily TSI fluxes (based on TSIS-1 TIM Version 3) were correctly scaled to the SORCE Version 15 reference and updated during February 2021. The EBAF product was impacted during August 2019 and May 2020 through July 2020. The resultant global averaged daily and monthly fluxes were found to be ~0.2 W m^{-2} too large out of a 20-year mean TSI flux of 339.88 W m^{-2}.
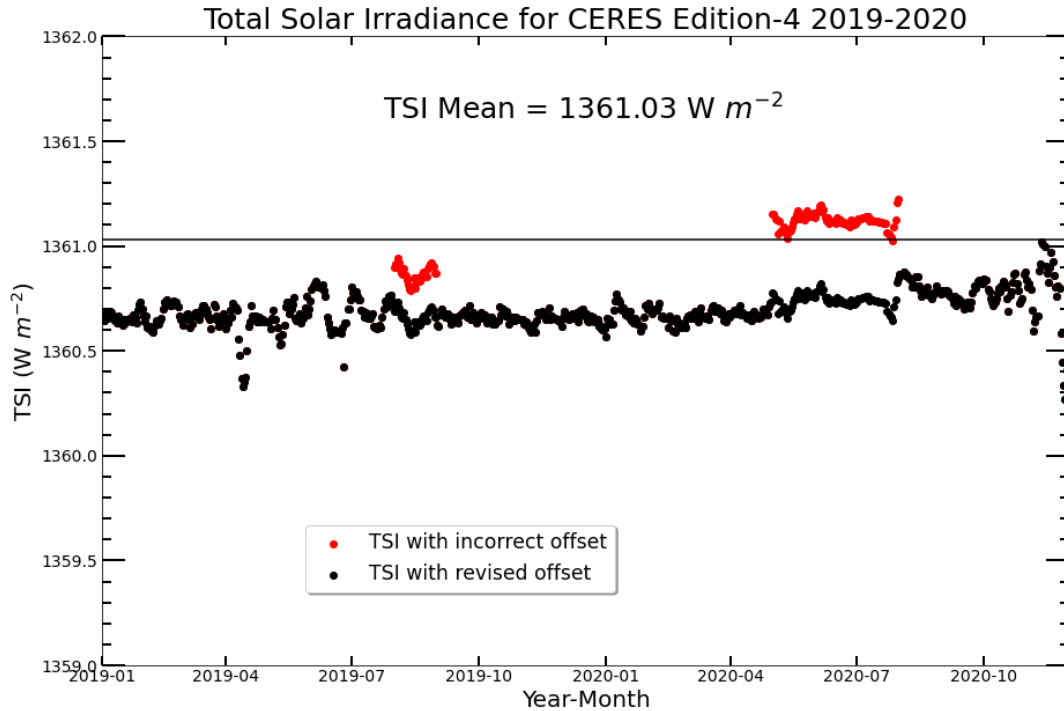
Figure 5-1. TSIS-1 TIM Version 3 at 1 AU incorrect scaling (red daily values) compared to the correct scaling (black daily values).

- In determining monthly mean cloud free area clear-sky SW TOA fluxes from daily mean values, the daily mean SW fluxes are weighted by the gridbox clear area fraction in order to minimize the influence of cloud contamination on the monthly mean clear-sky SW TOA flux. In contrast, daily mean clear-sky LW TOA fluxes are weighted equally when computing gridbox monthly mean values.

- Since TOA flux represents a flow of radiant energy per unit area and varies with distance from the earth according to the inverse-square law, a reference level is also needed to define satellite-based TOA fluxes. From theoretical radiative transfer calculations using a model that accounts for spherical geometry, the optimal reference level for defining TOA fluxes in radiation budget studies for the earth is estimated to be approximately 20 km. At this reference level, there is no need to explicitly account for horizontal transmission of solar radiation through the atmosphere in the earth radiation budget calculation. In this context, therefore, the 20-km reference level corresponds to the effective radiative "top of atmosphere" for the planet. Since climate models generally use a plane-parallel model approximation to estimate TOA fluxes and the earth radiation budget, they implicitly assume zero horizontal transmission of solar radiation in the radiation budget equation and do not need to specify a flux reference level. By defining satellite-based TOA flux estimates at a 20-km flux reference level, comparisons with plane-parallel climate model calculations are simplified since there is no need to explicitly correct plane-parallel climate model fluxes for horizontal transmission of solar radiation through a finite atmosphere. For a more detailed discussion of reference level, please see Loeb et al. (2002).

- When the solar zenith angle is greater than 90°, twilight flux (Kato and Loeb 2003) is added to the outgoing SW flux in order to take into account the atmospheric refraction of light. The magnitude of this correction varies with latitude and season and is determined independently for all-sky and clear-sky conditions. In general, the regional correction is less than 0.5 W m^{-2}, and the global mean correction is 0.2 W m^{-2}. Due to the contribution of twilight, there are regions near the terminator in which outgoing SW TOA flux can exceed the incoming solar radiation. Users should be aware that in these cases, albedos (derived from the ratio of outgoing SW to incoming solar radiation) exceed unity.

- EBAF uses geodetic weighting to compute global means. The spherical Earth assumption gives the well-known $S_O/4$ expression for mean solar irradiance, where S_O is the instantaneous solar irradiance at the TOA. When a more careful calculation is made by assuming the Earth is an oblate spheroid instead of a sphere, and the annual cycle in the Earth's declination angle and the Earth-sun distance is taken into account, the division factor becomes 4.0034 instead of 4. The following file provides the zonal geodetic weights used to determine global mean quantities.
(https://ceres.larc.nasa.gov/data/general-product-info/#geodetic-zone-weights-information).

- Starting with the data date of August 2021, a supplemental dataset used to fill gaps in the microwave snow and ice data within 50 km of coasts (including large lakes and seas) changed to a higher resolution product, resulting in differences in those snow/ice maps. Figure 5-2 shows differences due to this change in the all-sky and clear-sky TOA SW and LW fluxes from SSF1deg-Ed4A-Aqua run for January 2021. The differences are restricted to coastlines and are generally less than 5 W m^{-2}.
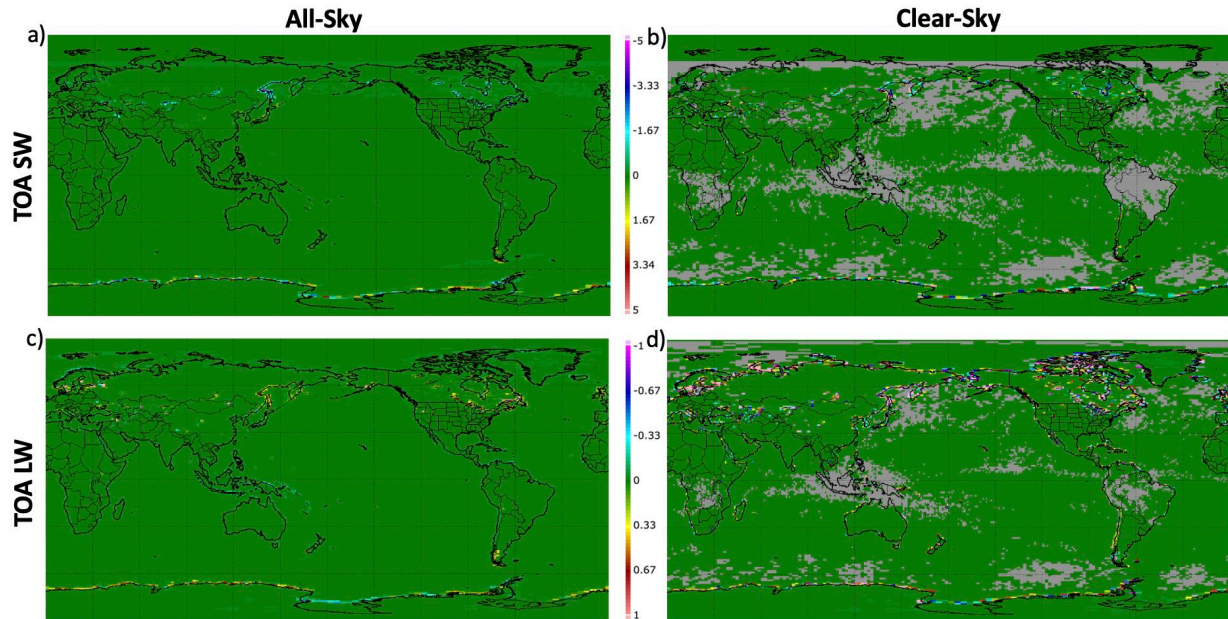

Figure 5-2. Differences in SSF1deg Ed4A monthly mean TOA fluxes (W m^{-2}) in January 2021 due to the change in the supplemental snow/ice dataset.

(b) <u>Cloud Properties:</u>

- EBAF Ed4.1 provides MODIS-based cloud properties (cloud fraction, daytime optical depth, effective pressure and effective temperature) from SSF1deg Ed4.1. For March 2000-June 2002, cloud properties are based upon MODIS Terra only (CERES_SSF1deg-Month_Terra-MODIS_Ed4A), whereas cloud properties for July 2002 onwards are given by the average of MODIS Terra and Aqua. No attempt is made to force consistency between the MODIS Terra and MODIS Aqua cloud properties. ***Therefore, cloud properties may exhibit a discontinuity in July 2002 owing to MODIS Terra and Aqua calibration differences and diurnal cloud property differences between the two periods.***
- Because the Aqua MODIS 1.6 μm channel failed shortly after launch, the 1.24 μm channel is used as an alternative in both Aqua and Terra Ed4.1 daytime cloud optical depth retrievals over snow. However, the 1.24 μm channel is not optimal for cloud optical depth since surface reflectance can affect retrievals more than the 1.6 μm channel. Surface shortwave downward flux validation of radiative transfer results over Dome C using 1.6 μm and 1.24 μm cloud retrievals anecdotally suggest that the 1.24 μm cloud optical depths over snow are too large by several percent.
- The Terra-MODIS water vapor (6.76-μm) and the 8.55-μm channels have degraded since 2008, leading to some artificial trends in cloud properties that are most significant over polar regions (day and night) and non-polar oceans (nighttime). Corrections were made after the Terra spacecraft anomaly event (February 18-28, 2016) in an attempt to restore these channels to pre-degradation levels. As a result, some cloud properties also exhibit a sharp discontinuity and inconsistency before and after the Terra spacecraft anomaly over Antarctica and the Arctic Ocean during daytime and nighttime, and over the non-polar oceans during nighttime. The TOA SW and LW fluxes are not significantly affected.

(c) <u>Surface Fluxes:</u>

- Cloud radiative effects are computed as all-sky flux minus clear-sky flux.
- The net flux is positive when the energy is deposited to the surface, i.e. the net is defined as downward minus upward flux.
- There are regions where the surface flux adjustments are large, such as over the Andes, Tibet, and central eastern Africa. As a result, the deseasonalized anomalies over these regions can be noisy.
- Because the degradation of Terra water vapor channels affected cloud retrievals starting around 2008, downward longwave flux anomalies over polar regions show a downward trend. Therefore, trend analyses with surface fluxes over polar regions from Ed4 EBAF-Surface should be avoided.
- Although the frequency of occurrence of a positive net shortwave cloud effect or a negative net longwave cloud effect is rare, they are not entirely absent when cloud free area clear-sky fluxes are used for the cloud effect calculation. A possible reason that these apparently unphysical cloud radiative effects occur is because of a mismatch of sampling between all-sky and clear-sky. For example, if clear-sky is sampled during daytime more often than during nighttime, the net clear-sky longwave flux is less negative than the net clear-sky longwave flux with a uniform sample throughout a month. Therefore, when the less negative clear-sky net longwave flux is subtracted from all-sky net longwave flux, which is also generally negative, the resulting net longwave cloud effect can be negative. For shortwave over polar region where

the solar zenith angle changes rapidly over the course of a month, if clear-sky samplings occur when solar zenith angle is large and a smaller net clear-sky shortwave flux is subtracted from all-sky net shortwave flux, the cloud effect can be positive.

- The MODIS-based cloud properties distributed within EBAF Ed4.1 are not exactly the same as those used for surface flux computations. Between 60°N and 60°S, cloud properties used in the surface flux calculations are derived from both MODIS and geostationary (GEO) imagers, which are only available in the SYN1deg Ed4.1 product. Surface fluxes poleward of 60° are computed using only MODIS-based cloud properties.

- To ensure surface and TOA fluxes are consistent, a bias correction and Lagrange multiplier processes is used to adjust the MODIS+GEO cloud properties within uncertainty to ensure flux computations at TOA are consistent with those observed at TOA. The surface flux is then recomputed using the adjusted cloud properties (see Kato et al., 2018 for more details).

- A larger number of input parameters are needed to determine surface fluxes in EBAF Ed4.1. As a consequence, surface fluxes are potentially vulnerable to input data artifacts. It is hard to determine whether a specific large surface flux anomaly is real or caused by artifacts. If it is caused by artifacts, it is even harder to determine what variables are responsible for the artifact. The standard deviation of deseasonalized anomalies and standard deviation of the difference of surface fluxes of two consecutive months provide useful metrics to detect artifacts. The size of flux anomalies depends upon spatial and temporal scales. Usually, a visual inspection of anomaly time series is enough to detect large anomalies. To make a quantitative decision, we provide two sets of standard deviations in Table 5-1 and Table 5-2. If one finds a flux anomaly larger than these standard deviations for similar temporal and spatial scale, one should be cautious about analyzing the anomaly or computing a trend with the anomaly. These values do not tell if the anomalies are real or artifacts. Anomalies greater than these values, however, need to have physical reasons for their large magnitude.

Table 5-1. Standard deviation of deseasonalized anomalies of fluxes averaged over three surface types in W m^{-2}. Numbers in parentheses are in percentage of the standard deviation relative to the mean.

	Global	Ocean	Land	Polar
All-sky				
SW down	0.78 (0.42)	1.00 (0.53)	1.35 (0.69)	1.83 (1.54)
SW up	0.29 (1.21)	0.22 (1.79)	0.54 (1.46)	2.20 (2.56)
LW down	1.07 (0.31)	1.02 (0.28)	1.69 (0.51)	2.91 (1.58)
LW up	0.78 (0.20)	0.66 (0.16)	1.45 (0.37)	2.68 (1.22)
Clear-sky				
SW down	0.50 (0.21)	0.55 (0.22)	0.80 (0.32)	1.07 (0.74)
SW up	0.34 (1.12)	0.26 (1.51)	0.68 (1.47)	2.37 (2.38)
LW down	1.01 (0.32)	0.90 (0.27)	1.70 (0.55)	2.05 (1.43)
LW up	0.78 (0.20)	0.68 (0.16)	1.44 (0.36)	2.70 (1.24)

Table 5-2. Standard deviation of the flux anomaly difference between two consecutive months averaged over three surface types in W m^{-2}.

	Global	Ocean	Land	Polar
All-sky				
SW down	0.91 (0.48)	1.25 (0.66)	1.75 (0.90)	2.09 (1.75)
SW up	0.24 (1.02)	0.17 (1.35)	0.56 (1.52)	1.95 (2.28)
LW down	0.59 (0.17)	0.55 (0.15)	1.38 (0.41)	3.67 (2.00)
LW up	0.42 (0.11)	0.21 (0.05)	1.34 (0.34)	3.26 (1.49)
Clear-sky				
SW down	0.48 (0.20)	0.55 (0.22)	0.84 (0.34)	1.24 (0.85)
SW up	0.28 (0.92)	0.21 (1.21)	0.68 (1.46)	2.23 (2.24)
LW down	0.50 (0.16)	0.41 (0.12)	1.41 (0.46)	2.49 (1.74)
LW up	0.42 (0.11)	0.23 (0.05)	1.38 (0.35)	3.06 (1.41)

- Replacements of existing geostationary satellites by newer geostationary satellites happen, introducing discontinuities in retrieved cloud properties. Almost all discontinuities occur at a regional scale. But some discontinuities are large in magnitude or affect a large region; also, multiple cloud properties may affect radiative fluxes systematically. Consequently, they can affect the global mean trend. Himawari-8 replaced MTSAT-2 on July 6, 2015, and GOES-16 replaced GOES-13 on January 1, 2018. These replacements introduced discontinuities in the downward longwave flux, which in turn affected the time series of global monthly anomalies (see Section 4.1 of the EBAF-Surface data quality summary for more details).

6.0   Accuracy and Validation

Table 6-1 provides an estimate of the uncertainty in the 1°×1° regional monthly mean TOA and surface radiative fluxes in EBAF Ed4.1. These correspond to the overall regional uncertainty when all 1°x1° latitude-longitude regions are considered. However, we expect SW uncertainties to be larger in certain locations, such as in high latitude regions over sea-ice off the coast of Antarctica and for regions over land with high aerosol loadings (e.g., eastern China). In the LW, regional uncertainties in clear-sky flux and CREs are larger at high latitudes due primarily to the greater challenge associated with clear-sky scene identification from passive sensors, particularly during polar night.

Table 6-1. Uncertainty in 1°×1° regional monthly TOA and surface fluxes and CREs for SW, LW, and net (W m^{-2}). Here, clear-sky is defined for the total region.

	TOA		
	All-Sky	Clear-Sky	CRE
SW	2.5	5.4	5.9
LW	2.5	4.6	4.5
NET	3.5	7.1	7.4
	Surface		
	All-Sky	Clear-Sky	CRE
LW down	9	8	9
LW up	15	15	17
LW Net	17	17	18
SW down	14	6	14
SW up	11	11	14
SW Net	13	13	16
SW + LW Net	20	21	26

6.1   TOA Flux Uncertainties

The methodology used to determine all-sky TOA flux uncertainties is described in detail in Loeb et al. (2018; Section 4). The uncertainty is determined by including all known sources of uncertainty and combining them assuming they are independent, so the total uncertainty is given by the square root of the sum-of-squares of the individual contributions. Sources of uncertainty include: instrument calibration, radiance-to-flux conversion error and diurnal corrections. The clear-sky TOA flux uncertainties in Loeb et al. (2018) correspond only to clear-sky fluxes determined for cloud-free portions of CERES footprints. Here we revisit the uncertainties, accounting for uncertainties in the Δ^C adjustments (Section 2.0) as well. We assume the regional uncertainty in the SW and LW Δ^C adjustments to be 2 W m^{-2} and 1 W m^{-2}, respectively, and assume these uncertainties are independent of other sources of uncertainty. The Δ^C adjustment

uncertainties are based upon the RMS differences between the Δ^C adjustments using SYN1deg and the following reanalyses: MERRA-2, ERA-Interim and ERA5 (see Loeb et al. 2020 for details).

Regional uncertainties in clear-sky SW and LW TOA flux are approximately 5 W m^{-2}, twice those for all-sky. The larger clear-sky uncertainty is due to the additional uncertainty associated with identifying cloud-free scenes using the MODIS imager. Uncertainties in regional monthly CREs are determined from all-sky, clear-sky and Δ^C adjustment uncertainties, accounting for the correlation in calibration uncertainty between all-sky and clear-sky (Loeb et al., 2018).

6.2   Surface Flux Uncertainties

Uncertainties in surface fluxes are discussed in detail in Kato et al. (2018; Section 4). Uncertainties are primarily determined by comparing EBAF surface fluxes with observations at surface sites over land and buoys over ocean. Overall, they find that mean biases are smaller than the uncertainty of surface observations. To estimate clear-sky downward flux uncertainty, we analyze coincident computed and measured surface fluxes at 36 ground sites and 46 ocean buoys for the period between March 2000 and October 2018. Land sites and ocean buoys are predominately located in the midlatitude and tropics, respectively (see Kato et al., 2018). Because clear-sky conditions do not persist for the entire month at any given site, we use hourly surface flux measurements that coincide with Terra and/or Aqua observation times. We select clear-sky fluxes based upon MODIS cloud fraction with a threshold of zero cloud cover over the grid box where each ground site is located. Land sites are separated into three regional groups, according to whether they are from the Atmospheric Radiation Measurement (ARM) program (Ackerman and Stokes, 2003), the surface radiation budget observing network (SURFRAD; Augustine et al. 2000) or the Baseline Surface Radiation Network (BSRN; Ohmura et al., 1998; Driemel et al., 2018). In the SW, there are between 3,000 and 5,000 matched pairs of computed and measured surface fluxes for all sites within a group (it is roughly double that for LW since LW includes nighttime as well). For each group, a bias and standard deviation is calculated from all matched pairs over the entire period. The monthly mean bias for a group is assumed equal to the bias of all matched pairs and the standard error in the monthly mean bias is calculated from the standard deviation of all matched pairs divided by the square-root of 30. The monthly mean bias and standard error are then divided by the overall mean of all matched pairs, and these are then multiplied by the global monthly mean land flux. This is equivalent to assuming the relative uncertainty is spatially and temporally constant. The root-mean-square difference (RMSD) between computed and measured fluxes for the group are determined from the square-root of the sum of the squares of the mean bias and standard error. This process is repeated for each land group, which are then combined by weighting their RMSDs by the number of sites in a group. The RMSD for ocean buoy sites is computed in the same way except that only one group is used because almost all buoys are located in tropics. The ocean and land RMSDs are then combined to determine a global RMSD by area-weighting the ocean and land values. Because the uncertainties in monthly mean downward surface LW and SW fluxes measured at the surface sites are both approximately 5 W m^{-2} (Michalsky et al. 1999; Gröbner et al. 2014), we add the surface measurement uncertainties in quadrature with the global RMSDs to estimate the overall SW and LW uncertainties.

The resulting regional uncertainties in clear-sky surface downward fluxes are 6 W m^{-2} for SW and 8 W m^{-2} for LW (Table 6-1). In the LW, the uncertainty for all-sky and clear-sky are comparable, but for SW the all-sky uncertainty is over a factor of 2 larger than clear-sky. For the

regional uncertainty in the clear-sky upward SW and LW fluxes, we assume that the uncertainty is the same as the all-sky uncertainty because the uncertainty in surface albedo, emissivity, and surface skin temperature are largely contributing the upward flux uncertainty.

Regional uncertainties in surface net flux, SW+LW flux, and CRE are determined by accounting for the upward and downward flux uncertainties and their covariance. We compute the latter using surface flux adjustments applied to computed fluxes when CERES-derived TOA fluxes are used to constrain surface fluxes. In the process, surface, atmosphere, cloud, and aerosol properties are adjusted to match computed TOA fluxes with TOA fluxes derived from CERES observations (Kato et al. 2018). Based on the adjustment of these properties, surface SW and LW upward and downward fluxes are also adjusted. Therefore, surface flux adjustments are considered to be the error in the surface fluxes due to errors in inputs used in the computation. Temporal error correlations are derived from regional surface flux adjustments averaged over the entire globe using the time period from March 2000 through February 2016. Regional uncertainties are 18 W m^{-2} for LW net downward flux, 16 W m^{-2} for SW net downward flux, and 26 W m^{-2} for SW+LW Net (Table 6-1).

7.0   Version History

May 2019: Produced Edition 4.1 EBAF. Edition 4.1 replaced Edition 4.0.

August 2019: Added clear-sky sampling corrections Δ^c.

June 2021: Applied correction to TOA upward and surface downward clear-sky longwave flux for the total region from November 2019 onward. The correction mitigates a spurious drift caused by the loss of a microwave humidity sounder in the GEOS-5.4.1 temperature and humidity reanalysis input data stream. The original release of November 2019 through November 2020 has been modified with the correction.

August 2021: Completed the revision (third released version) of the correction to TOA upward and surface downward flux for the total region from November 2019.

8.0   References

Ackerman, T. P., and G. M Stokes, 2003; The atmospheric radiation measurement program, *Physics Today*, **56**, doi: 10.1063/1.1554135.

Augustine, J. A., J. J. DeLuisi, and C. N. Long, 2000: SURFRAD –A national surface radiation budget network for atmospheric research. *Bull. Amer. Meteor. Soc.*, **81**, 2341–2358, doi:10.1175/1520-0477(2000)081<2341:SANSRB>2.3.CO;2.

Clarke, A. D., et al. (2002), INDOEX aerosol: A comparison and summary of chemical, microphysical, and optical properties observed from land, ship, and aircraft, *J. Geophys. Res.*, **107**(D19), 8033, doi:10.1029/2001JD000572.

Collins, W. D., P. J. Rasch, B. E. Eaton, B. V. Khattatov, J.-F. Lamarque, and C. S. Zender, 2001: Simulating aerosols using a chemical transport model with assimilation of satellite aerosol retrievals: Methodology for INDOEX. *J. Geophys. Res.*, **106**, 7313–7336.

Driemel, A., and Co-Authors, 2018: Baseline Surface Radiation Network (BSRN): structure and data description (1992–2017), *Earth Syst. Sci. Data*, **10**, 1491-1501, doi:10.5194/essd-10-1491-2018.

Gröbner, J., I. Reda, S. Wacker, S. Nyeki, K. Behrens, and J. Gorman, 2014: A new absolute reference for atmospheric longwave irradiance measurements with traceability to SI units. *J. Geophys. Res. Atmos.*, **119**, 7083–7090, doi:10.1002/2014JD021630.

Jin, Z., T. P. Charlock, W. L. Smith, Jr., and K. Rutledge, 2004: A look-up table for ocean surface albedo. *Geophys. Res. Lett.*, **31**, L22301.

Johnson, G. C., J. M. Lyman, and N. G. Loeb. 2016. Improving estimates of Earth's energy imbalance. *Nature Climate Change*, **6**, 639-640, doi:10.1038/nclimate3043.

Kato, S., and N. G. Loeb, 2003: Twilight irradiance reflected by the earth estimated from Clouds and the Earth's Radiant Energy System (CERES) measurements. *J. Climate*, **16**, 2646–2650.

Kato, S., F. G. Rose, D. A. Rutan, T. E. Thorsen, N. G. Loeb, D. R. Doelling, X. Huang, W. L. Smith, W. Su, and S.-H. Ham, 2018: Surface irradiances of Edition 4.0 Clouds and the Earth's Radiant Energy System (CERES) Energy Balanced and Filled (EBAF) data product, *J. Climate*, **31**, 4501-4527, doi:10.1175/JCLI-D-17-0523.1.

Loeb, N. G., K. J. Priestley, D. P. Kratz, E. B. Geier, R. N. Green, B. A. Wielicki, P. O. R. Hinton, and S. K. Nolan, 2001: Determination of unfiltered radiances from the Clouds and the Earth's Radiant Energy System (CERES) instrument. *J. Appl. Meteor.*, **40**, 822–835.

Loeb, N. G., S. Kato, and B. A. Wielicki, 2002: Defining top-of-atmosphere flux reference level for Earth Radiation Budget studies. *J. Climate*, **15**, 3301-3309.

Loeb, N. G., D. R. Doelling, H. Wang, W. Su, C. Nguyen, J. G. Corbett, L. Liang, C. Mitrescu, F. G. Rose, and S. Kato, 2018: Clouds and the Earth's Radiant Energy System (CERES) Energy Balanced and Filled (EBAF) Top-of-Atmosphere (TOA) Edition-4.0 data product. *J. Climate*, **31**, 895-918, doi: 10.1175/JCLI-D-17-0208.1.

Loeb, N. G., F. G. Rose, S. Kato, D. A. Rutan, W. Su, H. Wang, D. R. Doelling, W. L. Smith, Jr., and A. Gettelman, 2020: Towards a consistent definition between satellite and model clear-sky radiative fluxes. *J. Climate*, **33**, 61-75, doi: 10.1175/JCLI-D-19-0381.1.

Michalsky, J. J., E. Dutton, M. Rubes, D. Nelson, T. Stoffel, M. Wesley, M. Splitt, and J. DeLuisi, 1999: Optimal measurement of surface shortwave irradiance using current instrumentation. *J. Atmos. Oceanic Technol*., **16**, 55–69, doi:10.1175/1520-0426(1999)016<0055:OMOSSI>2.0.CO;2.

Minnis P., S. Sun-Mack, D. F. Young, P. W. Heck, D. P. Garber, Y. Chen, D. A. Spangenberg, R. F. Arduini, Q. Z. Trepte, W. L. Smith, Jr., J. K. Ayers, S. C. Gibson, W. F. Miller, G. Hong, V. Chakrapani, Y. Takano, K.-N. Liou, Y. Xie, and P. Yang, 2011: CERES Edition-2 cloud property retrievals using TRMM VIRS and Terra and Aqua MODIS data--Part I: Algorithms. *IEEE Trans. Geosci. Remote Sens*., **49**, 4374-4400.

Minnis, P., S. Sun-Mack, Y. Chen, F.-L. Chang, C. R. Yost, W. L. Smith, Jr., P. W. Heck, R. F. Arduini, S. T. Bedka, Y. Yi, G. Hong, Z. Jin, D. Painemal, R. Palikonda, B. R. Scarino, D. A. Spangenberg, R. A. Smith, Q. Z. Trepte, P. Yang, and Y. Xie, 2020: CERES MODIS cloud product retrievals for Edition 4, Part I: Algorithm changes. *IEEE Trans. Geosci. Remote Sens.*, **59**, 2744-2780, doi: https://doi.org/10.1109/TGRS.2020.3008866.

Ohmura, A., and Coauthors, 1998: Baseline Surface Radiation Network (BSRN/WCRP): New precision radiometry for climate research. *Bull. Amer. Meteor. Soc*., **79**, 2115–2136, https://doi.org/10.1175/1520-0477(1998)079<2115:BSRNBW>2.0.CO;2.

Rienecker, M. M. and Coauthors, 2008: The GOES-5 Data Assimilation System-Documentation of Versions 5.0.1, 5.1.0, and 5.2.0. NASA Tech. Rep. NASA/TM-2009-104606, Vol. 27, 118 pp.

Rutan, D. A., S. Kato, D. R. Doelling, F. G. Rose, L. T. Nguyen, T. E. Caldwell, and N. G. Loeb, 2015: CERES synoptic product: Methodology and validation of surface radiant flux. *J. Atmos. Oceanic Technol.*, **32**, 1121–1143, https://doi.org/10.1175/JTECH-D-14-00165.1.

Su, W., J. Corbett, Z. Eitzen, and L. Liang, 2015: Next-generation angular distribution models for top-of-atmosphere radiative flux calculation from CERES instruments: methodology. *Atmos. Meas. Tech*., **8**(2), 611-632. http://dx.doi.org/10.5194/amt-8-611-2015.

Trepte, Q. Z., P. Minnis, S. Sun-Mack, C. R. Yost, Y. Chen, Z. Jin, G. Hong, F.-L. Chang, W.,L. Smith, Jr., K. Bedka, T.L. Chee, 2019: Global cloud detection for CERES Edition 4 using Terra and Aqua MODIS data. *IEEE Trans. Geosci. Remote Sens.*, **57**, 9410-9449, doi: 10.1109/TGRS.2019.2926620.

Winker, D.M., and Co-authors, 2010: The CALIPSO Mission. A global 3D view of aerosols and clouds. *Bull. Amer. Met. Soc*., **91**, 1211-1230, DOI:10.1175/2010BAMS3009.1.

Yost, C., P. Minnis, S. Sun-Mack, Y. Chen, and W. L. Smith, Jr., 2020: CERES MODIS cloud product retrievals for Edition 4, Part II: Comparisons to CloudSat and CALIPSO. *IEEE Trans. Geosci. Remote Sens.*, **59**, 3695-3724, doi:10.1109/TGRS.2020.3015155.

9.0   Attribution

When referring to the CERES EBAF product, please include the data product and the data set version as "CERES_EBAF_Ed4.1."

The CERES Team has put forth considerable effort to remove major errors and to verify the quality and accuracy of this data. Please provide a reference to the following papers when you publish scientific results with the CERES EBAF_Ed4.1.

Loeb, N. G., D. R. Doelling, H. Wang, W. Su, C. Nguyen, J. G. Corbett, L. Liang, C. Mitrescu, F. G. Rose, and S. Kato, 2018: Clouds and the Earth's Radiant Energy System (CERES) Energy Balanced and Filled (EBAF) Top-of-Atmosphere (TOA) Edition-4.0 Data Product. *J. Climate*, **31**, 895-918, doi: 10.1175/JCLI-D-17-0208.1.
PDF available at https://journals.ametsoc.org/doi/pdf/10.1175/JCLI-D-17-0208.1

Kato, S., F. G. Rose, D. A. Rutan, T. E. Thorsen, N. G. Loeb, D. R. Doelling, X. Huang, W. L. Smith, W. Su, and S.-H. Ham, 2018: Surface irradiances of Edition 4.0 Clouds and the Earth's Radiant Energy System (CERES) Energy Balanced and Filled (EBAF) data product, *J. Climate*, **31**, 4501-4527, doi:10.1175/JCLI-D-17-0523.1.
PDF available at https://journals.ametsoc.org/doi/pdf/10.1175/JCLI-D-17-0523.1

When CERES data obtained via the CERES web site are used in a publication, we request the following acknowledgment be included: "These data were obtained from the NASA Langley Research Center CERES ordering tool at https://ceres.larc.nasa.gov/data/."

10.0 Feedback and Questions

For questions or comments on the CERES Data Quality Summary, contact the User and Data Services staff at the Atmospheric Science Data Center. For questions about the CERES subsetting/visualization/ordering tool at https://ceres.larc.nasa.gov/data/ please email LaRC-CERES-Help@mail.nasa.gov.

11.0   Document Revision Record

The Document Revision Record contains information pertaining to approved document changes. The table lists the Version Number, the date of the last revision, a short description of the revision, and the revised sections.

Document Revision Record

Version Number	Date	Description of Revision	Section(s) Affected
V1	06/08/2021	• Existing document put in version control.	All
V2	09/02/2021	• Replaced Figure 2-4 and adjusted text accordingly.	Sec. 2.1
V3	12/08/2021	• Added text and Figure 5-2 regarding change in snow/ice dataset.	Sec. 5.0